

On fitting the full spectrum of luminous red galaxies by using ULySS and STARLIGHT *

Gao-Chao Liu^{1,2,3}, You-Jun Lu¹, Xue-Lei Chen^{1,4}, Wei Du¹ and Yong-Heng Zhao¹

¹ Key Laboratory of Optical Astronomy, National Astronomical Observatories, Chinese Academy of Sciences, Beijing 100012, China; gcliu@nao.cas.cn

² University of Chinese Academy of Sciences, Beijing 100049, China

³ College of Science, China Three Gorges University, Yichang 443002, China

⁴ Center for High Energy Physics, Peking University, Beijing 100871, China

Received 2013 April 24; accepted 2013 May 10

Abstract We select a sample of quiescent luminous red galaxies (LRGs) from the Sloan Digital Sky Survey Data Release 7 with a high signal-to-noise ratio (S/N) to study the consistency of fitting the full spectrum by using different packages, mainly, ULySS and STARLIGHT. The spectrum of each galaxy in the sample is fitted by the full spectrum fitting packages ULySS and STARLIGHT. We find: (1) for spectra with higher S/Ns, the ages of stellar populations obtained from ULySS are slightly older than those from STARLIGHT, and metallicities derived from ULySS are slightly richer than those from STARLIGHT. In general, both packages can give roughly consistent fitting results. (2) For low S/N spectra, it is possible that the fitting by ULySS can become trapped at some local minimum in the parameter space during execution and thus may give unreliable results, but STARLIGHT can still give reliable results. Based on the fitting results of LRGs, we further analyze their star formation history and the relation between their age and velocity dispersion, and find that they agree well with conclusions from previous works.

Key words: galaxies: evolution — galaxies: formation — galaxies: stellar content

1 INTRODUCTION

Stellar population synthesis has been widely adopted to study distant galaxies and obtain various properties of galaxies. The method used by stellar population synthesis is to find a combination of a series of simple stellar populations (SSPs), for which the theoretical features can match the observational features of a galaxy (Crampin & Hoyle 1961). Usually, the best combination of SSPs can be found by matching the spectral energy distributions (SEDs), spectral line indices, or full spectrum of the combinations of SSPs with the observed ones. Fitting via SEDs depends on the shapes of continua and is seriously affected by dust extinction. By using spectral line indices, the strength or equivalent width (EW) of some obvious line features are found, but it is difficult to measure lines which are blended with other lines due to the effect of Doppler line broadening, particularly for low-resolution spectra. The full spectrum fitting method takes advantage of all available information

* Supported by the National Natural Science Foundation of China.

contained in a spectrum, including both the continuum and line features. A fitting method that uses a full spectrum can be applied by using different techniques, such as ULYSS and STARLIGHT. It is interesting to check whether the fitting results rely on the choice of the fitting package or not. In this paper, we investigate the differences, if any, between the two fitting packages that use the full spectrum, i.e., ULYSS and STARLIGHT, by fitting spectra of a sample of quiet luminous red galaxies (LRGs). We also use the results to further study the physical properties of LRGs.

2 SAMPLE SELECTION

The Sloan Digital Sky Survey (SDSS) is one of the most ambitious and influential surveys in the history of astronomy. It has already completed its two phases of operation (SDSS-I, 2000–2005; SDSS-II, 2005–2008) and obtained deep, multi-color images covering more than a quarter of the sky and has also derived high-quality spectra of a portion of the observed objects. The third phase of operation (SDSS-III, 2008–2014) is currently ongoing. The SDSS uses a dedicated 2.5-meter telescope at Apache Point Observatory, New Mexico, equipped with two powerful special-purpose instruments. The spectrographs used in SDSS-I and SDSS-II were fed by 640 optical fibers with a 3'' entrance aperture and the one in SDSS-III is fed by 1000 fibers with a 2'' aperture. The SDSS project has released its data periodically and in this paper we use data from SDSS DR7 released in July, 2008 (Abazajian et al. 2009).

In addition to the main galaxy sample, LRGs have also been important targets for the SDSS-I and SDSS-II surveys. On the one hand, LRGs are supposed to be passively evolving galaxies, so they have simple and pure stellar populations and their spectra can be fitted by SSPs. On the other hand, a large sample of LRGs can be obtained because they are bright sources. According to the selection criteria mentioned in Liu et al. (2012), we pick out a sample of LRGs which satisfy the following criteria to test the two stellar population synthesis packages.

- (1) We select galaxies with the “TARGET-GALAXY-RED” flags which mark those LRGs selected by the algorithm in Eisenstein et al. (2001) from the SDSS database. In this paper, we only choose LRGs that satisfy CUT I ($z < 0.4$).
- (2) In order to ensure the reliability of the fitting results, we confine the spectroscopic signal-to-noise (S/N) in the r -band to be greater than 25. We also select LRGs with spectroscopic $S/N > 10$ in the r -band in order to check the effects of S/N on the fitting results.
- (3) We apply more strict constraints to our sample. We require the SpecClass EQ ‘SPEC-GALAXY’ to make sure that the object is a true galaxy, zStat EQ ‘XCORR-HIC’ to make sure that the spectroscopic redshift of the galaxy is from the cross-identification between spectra and templates, zWarning EQ 0 to make sure that the redshift value is correct, $eClass < 0$ to make sure that it is composed of old stellar populations, $z < 0.4$ and $fracDew_r > 0.8$ to make sure that its surface brightness profile can be well fitted by the de Vaucouleurs profile.

We obtain a sample of 27 695 LRGs from SDSS DR7 that satisfy the above criteria. In order to just use simple stellar populations during the fitting, we need to, above all, ensure that the galaxies in our LRG sample are completely evolved. Therefore, we derive fluxes of several spectral lines ($H\alpha$ and [OII]) from the published MPA-JHU value-added catalogs¹ for all galaxies in our sample and then by further selection we obtain 3452 spectra with no emissions in $H\alpha$ or [OII] within the $2\text{-}\sigma$ level. To obtain a sample with well-distributed properties, we select the velocity dispersions, which are indicators of galaxy mass, for each galaxy in the 3452-galaxy sample from the MPA-JHU value-added catalogs and select galaxies with velocity dispersions between 200 and 320 km s^{-1} to be our final sample. Since there are only 52 galaxies with velocity dispersions greater than 320 km s^{-1} , we disregard these 52 galaxies. Hence, our final sample is composed of 2440 LRGs, which are divided into four sub-samples listed in Table 1 in terms of a velocity dispersion interval of 30 km s^{-1} .

¹ <http://www.map-garching.mpg.de/SDSS/DR7/raw-data.html>

Table 1 Quantities of LRGs in Each Sub-sample of LRGs

Sample	σ_v (km s ⁻¹)	Median redshift	Median absolute magnitude (<i>r</i> band)	Number
Sub-sample I	200 < σ_v ≤ 230	0.08	-20.96	791
Sub-sample II	230 < σ_v ≤ 260	0.11	-21.41	899
Sub-sample III	260 < σ_v ≤ 290	0.13	-21.70	553
Sub-sample IV	290 < σ_v ≤ 320	0.14	-21.90	197
Total	200 < σ_v ≤ 320	0.11	-21.40	2440

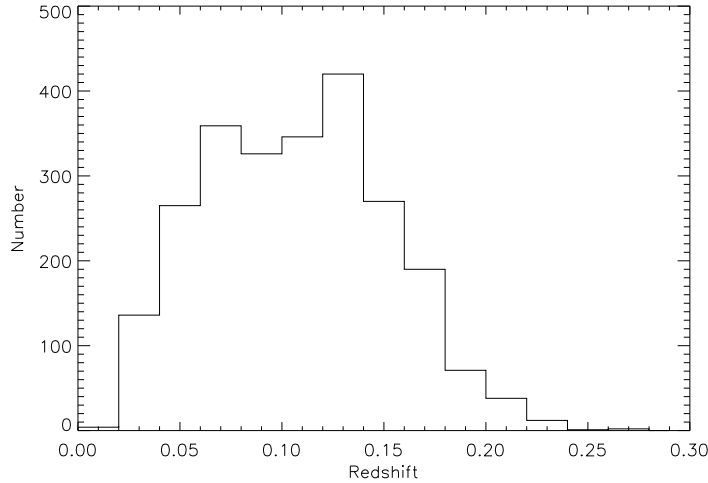
**Fig. 1** The redshift distribution of the LRGs.

Figure 1 shows the redshift distribution of our sample. We can see that the redshifts with high S/N in the spectra ($S/N > 25$) only account for less than 0.25 of our sample.

3 FITTING METHODS

3.1 ULySS

ULySS (University of Lyon Spectroscopic analysis Software; Koleva et al. 2009) is an open-source software package written in the GDL/IDL language by a team at Lyon University, France to analyze astronomical data. It has been freely available since 2009. ULySS has two powerful functions: (1) it is automatically able to estimate stellar atmospheric parameters (effective temperature- T_{eff} , surface gravity- $\log g$, metallicity-[Fe/H]) and radial velocity (R_V) of stars. (2) It can be used to study stellar populations, star formation histories and chemical enhancement histories of galaxies and star clusters. As a stellar population synthesis tool, ULySS fits the full spectrum of a stellar system with a linear combination of multiple simple stellar populations (SSPs). By minimizing χ^2 of the fitting, it resolves the most probable SSPs and relevant physical properties of the galaxy. An observational spectrum can be expressed as a weighted (W) linear combination of k non-linear components (CMPs) convolved with a line-of-sight velocity distribution (LOSVD), multiplied by a polynomial

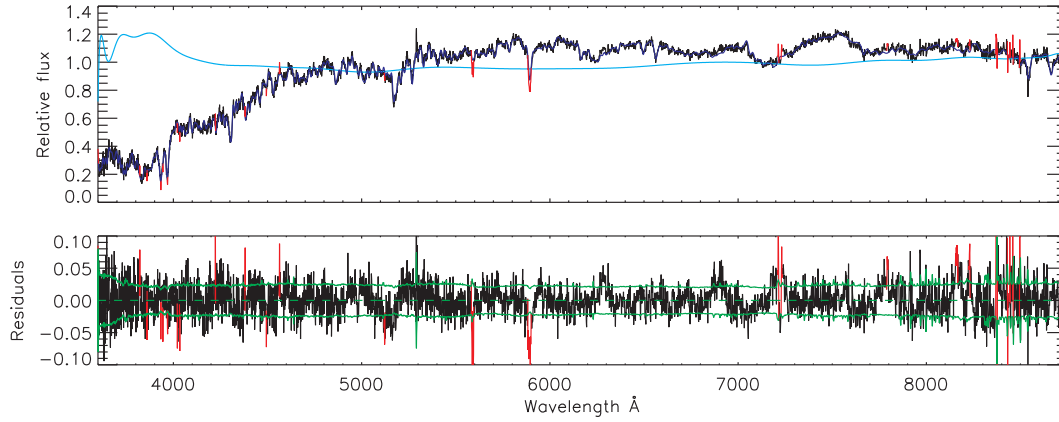


Fig. 2 The fitting for the spectrum spSpec-51868-0441-177.fit by ULySS. In the top panel, the black and blue lines represent the original spectrum and the best fit, respectively, and the cyan line represents the multiplicative n th-order polynomial that absorbs the effects of the imprecise flux calibration and the Galactic extinction. The pixels in the red region are masked in the fitting. The bottom panel shows the residual spectrum of the best fit and the green lines represent the $1\text{-}\sigma$ level.

continuum (n th-order polynomials) and added with another polynomial ($Q_m(\lambda)$), i.e.,

$$F_{\text{obs}}(\lambda) = P_n(\lambda) \times \left(\text{LOSVD}(v_{\text{sys}}, \sigma, h3, h4) \otimes \sum_{i=0}^{i=k} W_i \text{CMP}_i(a_1, a_2, \dots, \lambda) \right) + Q_m(\lambda), \quad (1)$$

where LOSVD is a function of the systematic velocity, v_{sys} , the velocity dispersion, σ , and perhaps a Gauss-Hermite expansion ($h3$ and $h4$), where λ is the logarithm of the wavelength. The CMP_i has different expressions for different problems. For example, if ULySS is used to study stellar atmospheric parameters, CMP_i will be a function of T_{eff} , $\log g$ and $[\text{Fe}/\text{H}]$. If ULySS is used to study stellar populations of galaxies or star clusters, CMP_i will be a function of age, $[\text{Fe}/\text{H}]$ and $[\text{Mg}/\text{Fe}]$. The n th-order polynomial, $P_n(\lambda)$, absorbs the effects of imprecise flux calibration and Galactic extinction, which is determined by ordinary least-squares at each evaluation of the function minimized by the Levenberg-Marquardt routine and we cannot decide the shape of $P_n(\lambda)$ before the spectral fitting. The additive polynomial, $Q_m(\lambda)$, is certainly more subtle to use, and is, in most cases, unnecessary. The ULySS package uses the full spectrum instead of only some characteristic spectral lines to avoid errors due to measurements of only individual lines and also avoids degeneracies between the fitting results of some physical parameters by simultaneously estimating the required parameters. ULySS also introduces a Line-Spread-Function (LSF) that matches the resolution of the observational spectrum to that of the model spectrum by injecting the relative LSF into either the model spectrum or observational spectrum. A spectrum (spSpec-51868-0441-177.fit) from our sample is shown as an example in Figure 2 to show the fitting by ULySS.

3.2 STARLIGHT

STARLIGHT (Cid Fernandes et al. 2004) is one of the most powerful tools for stellar population studies and is widely used in the field of early-type galaxies, late-type galaxies, star clusters, and

active galactic nuclei. STARLIGHT fits an observational spectrum with a model spectrum, M_λ , which is a combination of N_* SSPs with different ages and metallicities defined subjectively by users. M_λ can be expressed as follows

$$M_\lambda = M_\lambda(\mathbf{x}, A_V, v_*, \sigma_*) = \sum_{j=1}^{N_*} x_j \gamma_{j,\lambda} r_\lambda, \quad (2)$$

where $\gamma_{j,\lambda} \equiv b_{\lambda,j} \otimes G(v_*, \sigma_*)$, $b_{\lambda,j} \equiv \left(\frac{B_{\lambda,j}}{B_{\lambda_0,j}}\right)$ refers to the normalized flux of the j th observational spectrum, $B_{\lambda,j}$ refers to the flux of the j th model spectrum, $B_{\lambda_0,j}$ is the flux of the j th normalized model spectrum at the wavelength λ_0 , at which the flux has been used to normalize the full model spectrum, and $G(v_*, \sigma_*)$ describes the stellar movement in the radial direction and is expressed by a Gaussian function with a center at v_* and a width of σ_* . $r_\lambda \equiv 10^{-0.4(A_\lambda - A_V)}$ represents the global extinction. The x_j ($j = 1; \dots; N$), as one of the most significant parameters among all STARLIGHT outputs, represents the fraction contributed to the SSP component, with equivalent age t_j and metallicity Z_j , to the flux of the model spectrum at the normalization wavelength $\lambda_0 = 4020 \text{ \AA}$. Similarly to x_j , μ_j stands for the fraction contributed to stellar mass. The core algorithms of STARLIGHT include the Simulated Annealing Algorithm and the Metropolis Algorithm of the Markov Chain Monte Carlo Method, which search for the optimized parametric results in the whole parameter space to minimize the χ^2 value. The χ^2 can be expressed as $\chi^2 = \sum_\lambda [(O_\lambda - M_\lambda)w_\lambda]^2$, where w_λ^{-1} represents errors of the observational spectrum. According to formulas

$$\langle \log t_* \rangle_L = \sum_{j=1}^{N_*} x_j \log t_j, \quad (3)$$

$$\langle \log t_* \rangle_M = \sum_{j=1}^{N_*} \mu_j \log t_j, \quad (4)$$

and

$$\langle Z \rangle_L = \sum_{j=1}^{N_*} x_j z_j \quad (5)$$

we can obtain light-weighted age and metallicity of the galaxy. Figure 3 shows the fitting of the same spectrum as that shown in Figure 2 computed with STARLIGHT.

3.3 Template Library

There are a variety of template spectral libraries for evolutionary stellar population synthesis, such as BC03, Ma05, GALEV, GRASIL, Vazdekis/Miles and so on. Chen et al. (2010) used STARLIGHT to investigate the effect of the choice of different template libraries on stellar population synthesis and found that there are still some differences in the output between these different template libraries. In this paper, in order to compare the differences between two individual packages, we use the popular template library, BC03 (Bruzual & Charlot 2003), during the whole fitting process. The BC03 model has 6900 points in wavelength from $91 \text{ \AA} \sim 160 \text{ \mu m}$, 221 points in age from $0 \sim 20 \text{ Gyr}$, and 6 points in metallicity of 0.0001, 0.0004, 0.004, 0.008, 0.02 and 0.05. An SSP spectrum in BC03 is generated from the stellar spectral library, SteLib, and has a resolution of $\text{FWHM} = 3 \text{ \AA}$ in the optical wavelength range from 3200 \AA to 9500 \AA . In our work, we choose the Chabrier Initial Mass Function (IMF) (Chabrier 2003) and Padova94 (Bertelli et al. 1994) stellar evolutionary tracks.

We list the main parameters of BC03 in Table 2.

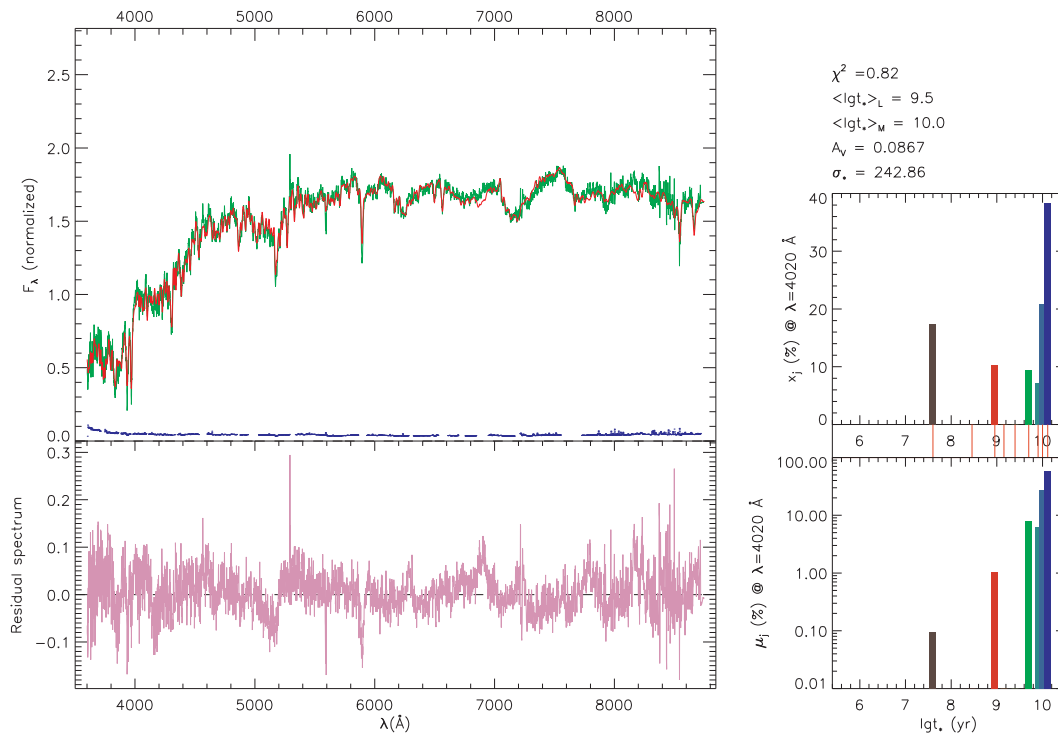


Fig. 3 The fitting for the spectrum spSpec-51868-0441-177.fit by STARLIGHT. In the upper left, the green represents the original spectrum, the red denotes the best-fit spectrum, and the blue shows the errors in which the missing place is not used to fit. The bottom left panel shows the residual spectrum of the best fit. The plots in the upper right and the bottom right respectively exhibit the light fraction (x_j) and mass fraction (μ_j) of individual stellar populations. The middle grid between the two plots in the right shows ages of the SSPs.

Table 2 Main Parameters of the BC03 Model

Model	Stellar library	Resolution (Å)	Wavelength (Å)	Age (Gyr)	Metallicity (dex)	IMF	Stellar evolutionary track
BC03	SteLib	3	3200–9500	0.1–20	−2.3–0.4	Chabrier	Padova 94

When using STARLIGHT, users need to choose SSPs with required ages and metallicities from the model. Since LRGs are regarded as old, metal-rich galaxies, we choose nine values of age (4, 286, 900 Myr, 1.4, 2.5, 5, 8, 10, 13 Gyr) and three values of metallicity (0.004, 0.02, 0.05) to construct 27-SSP model spectra so as to decrease the uncertainty of the fitting results which would increase with the numbers of SSPs we use. The choice of age and metallicity values of the base spectrum must cover all of the possible values in the parameter space of the sample studied and, at the same time, the number of base spectra must be as small as possible to reduce uncertainty in the fitting results. We also choose 10 values of age (i.e. 4, 286, 900 Myr, 1.4, 2.5, 5, 7, 9, 11, 13 Gyr) and four values of metallicity (i.e. 0.004, 0.008, 0.02, 0.05) to construct 40-SSP model spectra to fit the spectra of our sample, but the fitting results only change slightly. The direct fitting results of STARLIGHT include the contribution to light (x_j) and mass (μ_j) of every SSP and extinction, but in the ULySS package,

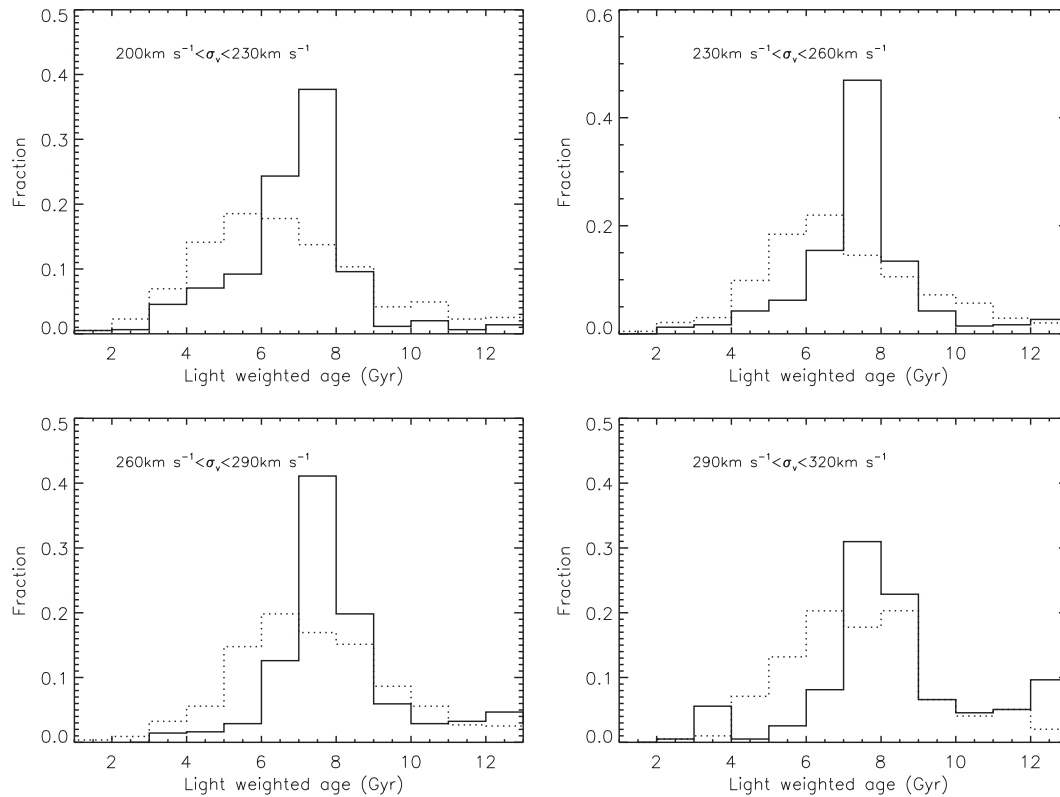


Fig. 4 Distributions of the light-weighted ages of LRGs. Solid and dashed lines represent results obtained from ULYSS and STARLIGHT, respectively.

it assembles all SSP spectra of BC03 into a FITS file with dimensions $5979 \times 116 \times 6$, where 5979, 116 and 6 respectively refer to the number of flux pixels in every SSP spectrum, the number of age points and the number of metallicity points. Other points can be obtained by interpolation between the grid points. Once fitted, STARLIGHT and ULYSS will both automatically search for the closest model spectrum to the observational spectrum and give the fitting results.

4 COMPARISON OF RESULTS

The spectrum of each LRG in our sample has been fitted by both STARLIGHT and ULYSS. In this section, we compare the results obtained from ULYSS with those from STARLIGHT and check whether or not the two methods give consistent results.

4.1 Age Distribution

Since ULYSS can only give light-weighted ages for resulting SSPs, we just take the light-weighted ages from STARLIGHT results, although STARLIGHT can additionally give the mass-weighted ages for resulting SSPs. Figure 4 shows the distributions of the SSPs' light-weighted ages derived from ULYSS (solid lines) and STARLIGHT (dashed lines) for the four sub-samples.

Table 3 Mean Light-weighted Ages of LRGs

Sub-sample	Mean age from STARLIGHT (Gyr)	Mean age from ULySS (Gyr)
Sub-sample I	6.7 ± 2.4	7.0 ± 1.9
Sub-sample II	7.1 ± 2.3	7.6 ± 1.8
Sub-sample III	7.6 ± 2.3	8.3 ± 2.0
Sub-sample IV	7.6 ± 2.1	8.6 ± 2.4

Table 4 Mean Metallicities of LRGs

Sub-sample	Mean metallicity from STARLIGHT (dex)	Mean metallicity from ULySS (dex)
Sub-sample I	0.12 ± 0.09	0.16 ± 0.04
Sub-sample II	0.15 ± 0.08	0.17 ± 0.04
Sub-sample III	0.16 ± 0.08	0.18 ± 0.04
Sub-sample IV	0.16 ± 0.07	0.20 ± 0.05

For all of the four sub-samples shown in Figure 4, the light-weighted ages of the LRGs derived from STARLIGHT are slightly younger than those derived from ULySS. In addition, both results from STARLIGHT and ULySS suggest that the sub-sample of LRGs with a larger velocity dispersion (σ) has larger ages. This conclusion agrees with the “downsizing” formation of the galaxies, which means that the more massive a galaxy is, the earlier it would have started to form. We tabulate the means and standard deviations of the light-weighted ages derived from STARLIGHT and ULySS for the four sub-samples of LRGs (in Table 3).

4.2 Metallicity Distribution

We compare distributions of LRG metallicities derived from STARLIGHT and ULySS in Figure 5. We can conclude that the majority of LRGs have richer metallicities than the Sun, which is in accord with our previous knowledge of LRGs being metal-rich galaxies. Although ULySS gives slightly higher metallicities than STARLIGHT, results from the two packages are generally consistent with each other. We tabulate the means and standard deviations of the light-weighted metallicities derived from STARLIGHT and ULySS for the four sub-samples of LRGs (in Table 4).

4.3 Effects of S/N on Fitting Results

In the analysis above, S/N values of our sample are greater than 25. In order to check the effect of S/N on fitting results from the two packages, we take a sample of LRGs with $S/N > 10$ by using the same selection criteria as those in Section 2, but lower the spectral S/N limit to 10. Then, similar to what we have done in Section 2, this sample is divided into four sub-samples in terms of velocity dispersion, which, respectively, have 4756, 8748, 7149 and 3230 LRGs. We only consider results of the first sub-sample as an example to demonstrate whether spectral S/N values influence the fitting results, as conclusions from checks on the other three sub-samples are completely the same as those from the first sub-sample. We previously showed the ages from the ULySS fitting for the first sub-sample with $S/N > 25$ (Sample-25; solid line) and currently with $S/N > 10$ (Sample-10; dashed line) in the upper left panel in Figure 6. From this plot, we discover that Sample-10 has two age peaks at nearly 3 Gyr and 7 Gyr. We carefully check the fitting processes for spectra having 3 Gyr peaks by performing 500 Monte Carlo simulations and finally find that the ULySS algorithms for these spectra have all become trapped in local minima of the parameter space. Because of the ease of becoming trapped in the local minima of parameter space, ULySS provides additional tools of Monte Carlo

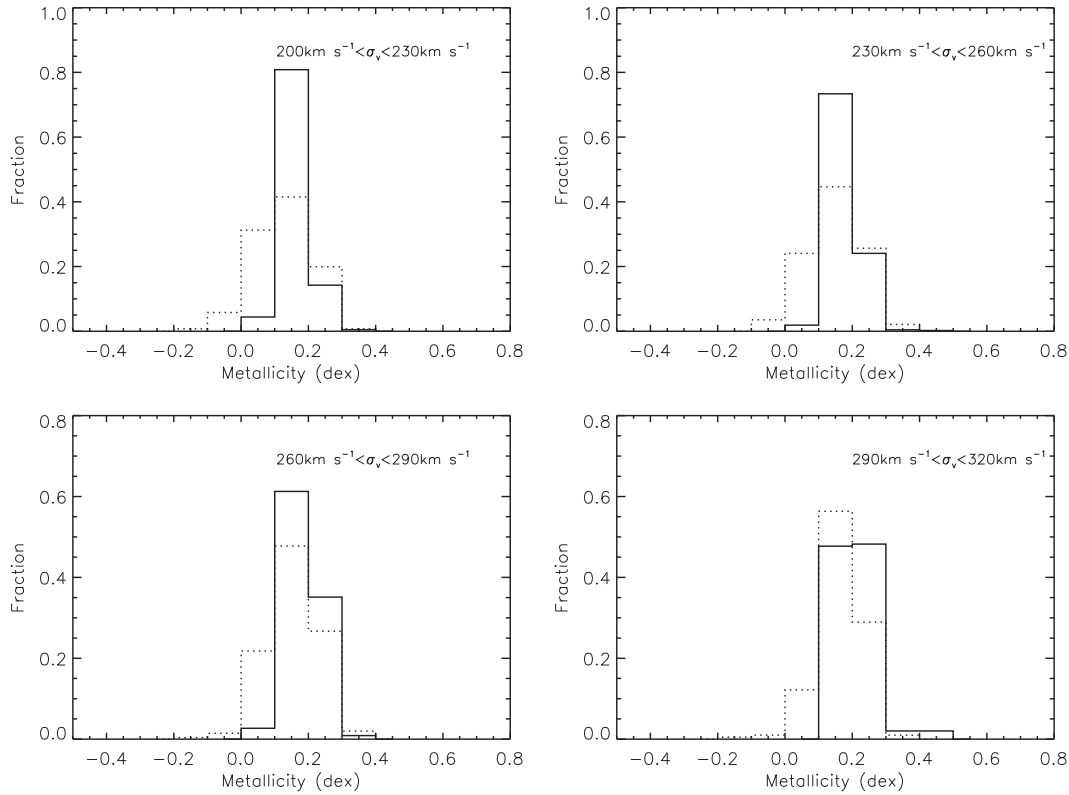


Fig. 5 Metallicity distribution of LRGs for the four sub-samples. The solid and dashed lines represent the results obtained from ULYSS and STARLIGHT, respectively.

simulations, χ^2 maps and convergence maps to explore parameter space and check the reliability of its fitting solutions. Combining our test and its characteristics, ULYSS may be more appropriate for spectra with high S/N, but if ULYSS is used for spectra with low S/N, the results must be carefully checked by the provided tools (Monte Carlo simulations, χ^2 maps and convergence maps) to see whether the fitting has become trapped in local minima of the parameter space. Similarly, we show the results from the STARLIGHT fitting in the upper right panel in Figure 6, which indicates a conclusion consistent with that from ULYSS. We show the effect of S/N on metallicities derived from the two packages in the bottom panels in Figure 6, from which we conclude from the fitting that spectral S/N has little effect on the metallicity.

5 VALIDATION OF FITTING METHODS

According to the above comparisons, we find that ULYSS and STARLIGHT give quantitatively different fitting results, though the general trends of the obtained age distribution and metallicity distribution are roughly consistent with each other for those spectra with high S/Ns. Which one is better? To answer this question, we carry out Monte Carlo simulations with a series of known inputs, and then compare the outputs from the two fitting codes with these inputs to address which code yields more reliable results. To do this, we select a series of model spectra from the BC03 template library, with the ages of model spectra being 1 to 13 Gyr with a step of 1 Gyr and the

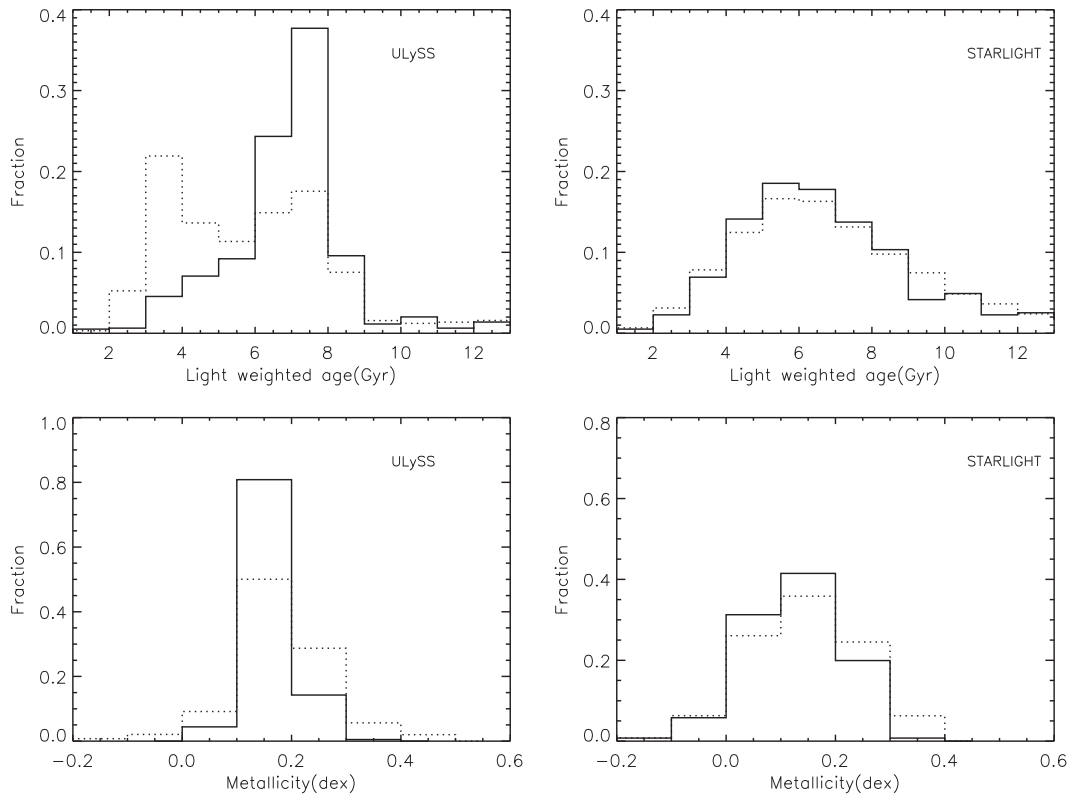


Fig. 6 Effects of S/N on the fitting results. Top panels show the age distribution obtained by using ULYSS (*left*) and STARLIGHT (*right*) to fit those LRGs with $S/N > 25$ (*solid lines*) and $S/N > 10$ (*dashed lines*). The bottom panels show the metallicity distributions.

metallicities being 0.0001, 0.0004, 0.004, 0.008, 0.02 and 0.05. We select a total of 13×6 model spectra as our test sample. We assign the error spectra from our model whose amplitude equals the flux of the model spectra divided by S/N and the error spectra follow a Gaussian distribution. Here, we assume $S/N=25$. Next, we fit these model spectra with both ULYSS and STARLIGHT. The fitting is made from 3900 \AA to 8500 \AA , which is similar to the wavelength coverage of our sample of LRGs.

ULySS uses the Levenberg-Marquardt routine to search the parameter space for the minimum of χ^2 , and it needs some initial estimated value (IEV) to begin searching the parameter space. We find the IEV is crucial for the final fitting results.

Figure 7 shows how the fitting results depend on the IEV. Panels (a) and (d) show the ages and metallicities derived from the ULYSS fitting when IEV of metallicities are equal to those input for the model spectra. We find that the outputs are almost the same as the inputs. Panels (b) and (e) show the outputs when IEVs of metallicities are equal to 0 dex. We find the outputs of those spectra with low metallicity (i.e. -2.3 , -1.7 , -0.7) are far from the inputs, but the outputs of those spectra around solar metallicity are very consistent with the inputs. We also test the situation when IEVs of metallicities are equal to -0.7 dex and Panels (c) and (f) show the results, which are similar to Panels (b) and (e). We also find the age and metallicity derived from fitting are anti-correlated by comparing the outputs of age with those of metallicity; that is, if we overestimate the metallicity then the age will be underestimated.

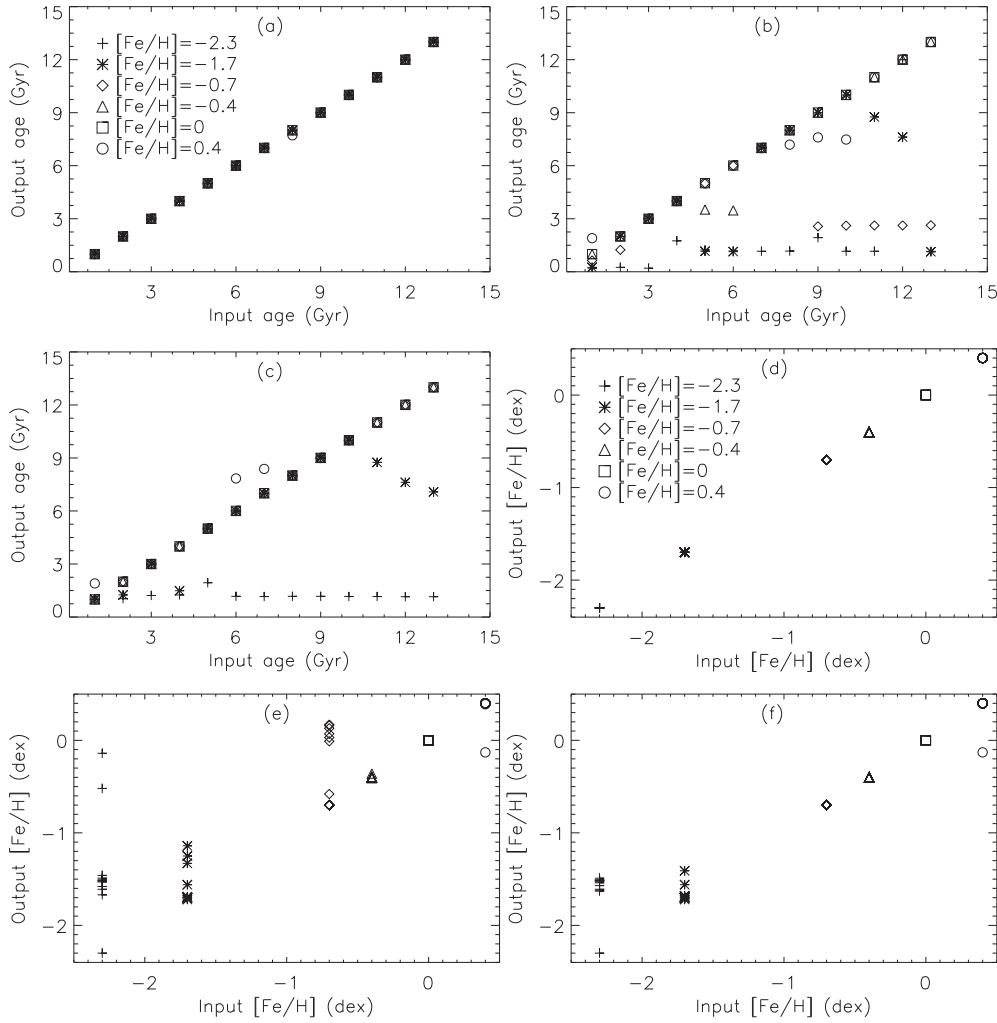


Fig. 7 Dependence of the fitting results on the IEV for ULySS. Panels (a), (b) and (c) show the fitting age of the model spectrum when the IEV of metallicities is equal to the inputs of the model spectra, the IEV of metallicity is equal to 0 dex and the IEV of metallicity is equal to -0.7 dex, respectively. Panels (d), (e) and (f) show the corresponding fitted metallicity of the model spectrum. The x -axis represents the inputs and the y -axis represents the outputs. The plus symbols, asterisks, diamonds, triangles, squares and circles represent the fitting results of model spectra with six different metallicities from low to high, respectively.

For STARLIGHT, we need to predefine the base spectra. We choose eight values of age (500 Myr, 1, 3, 5, 7, 9, 11, 13 Gyr) and six values of metallicity (0.0001, 0.0004, 0.004, 0.008, 0.02, 0.05) to construct 48-SSP model spectra. We also choose eight values of age and one value of metallicity to fit the model spectra with the same metallicity as our chosen value.

Figure 8 shows the fitting results. Panels (a) and (c) show the fitting results of age and metallicity with 8-SSP model spectra, respectively. Correspondingly, Panels (b) and (d) show the results with 48-SSP model spectra. From Figure 8, we can find the fitting results are stable and robust by adopting

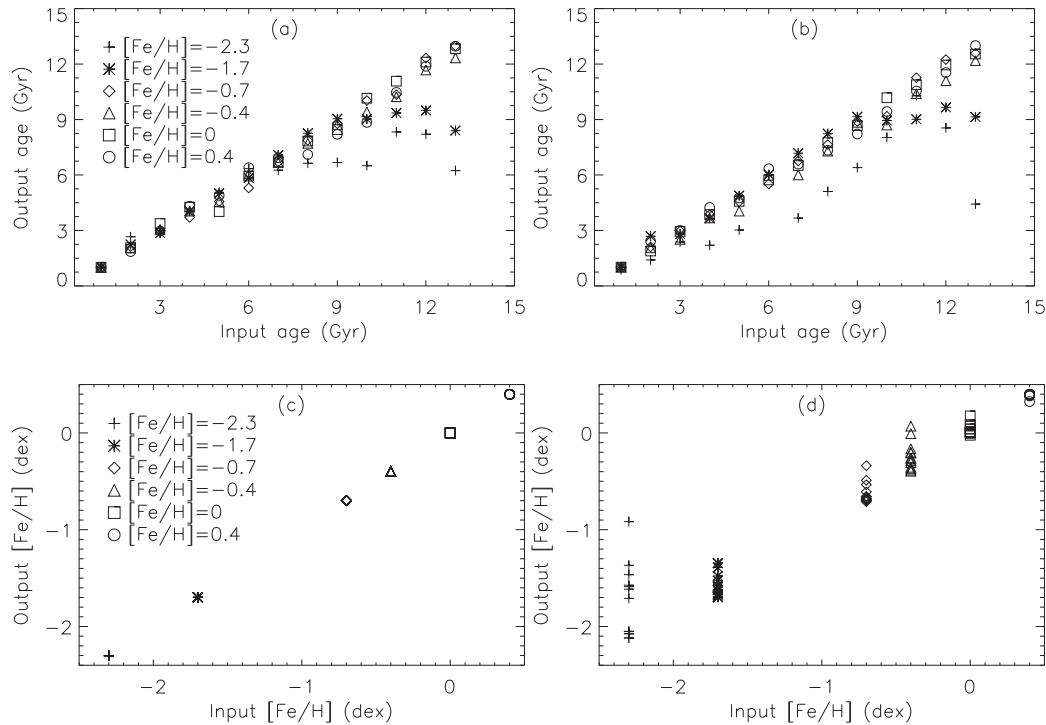


Fig. 8 Fitting results with STARLIGHT. Panels (a) and (c) show the fitting results of age and metallicity with 8-SSP model spectra, respectively; Panels (b) and (d) show the corresponding results with 48-SSP model spectra. The x -axis represents the inputs and the y -axis represents the outputs. The plus symbols, asterisks, diamonds, triangles, squares and circles represent the fitting results of model spectra with six different metallicities from low to high, respectively.

either 8-SSP model spectra or 48-SSP model spectra, though the outputs of age are systemically slightly younger than the inputs. The spectra with very low metallicity also cannot be well fitted, which could be caused by the limitation of the BC03 library since the model spectra with $[Fe/H] = -1.7$ and $[Fe/H] = -2.3$ are all computed from a very small sample of stars whose metallicity spans a large range, which lead to less accurate metallicity for model spectra.

On the whole, ULySS and STARLIGHT all can give consistent outputs compared with inputs for those spectra around solar metallicity and the fitting results derived from STARLIGHT are more stable and robust than those from ULySS, since the fitting results derived from ULySS show some dependence on the IEV.

6 PROPERTIES OF LRGs

By analyzing a sample of LRGs with both ULySS and STARLIGHT, we draw a conclusion that the two packages are able to give generally consistent fitting results, although the ages and metallicities derived from ULySS seem to be a little older and richer than those derived from STARLIGHT. It is worth noting that the results should be carefully checked to avoid being trapped in local minima of the parameter space when ULySS is used for low S/N spectra. Based on the parameters derived above, we will study some physical properties of LRGs in this section.

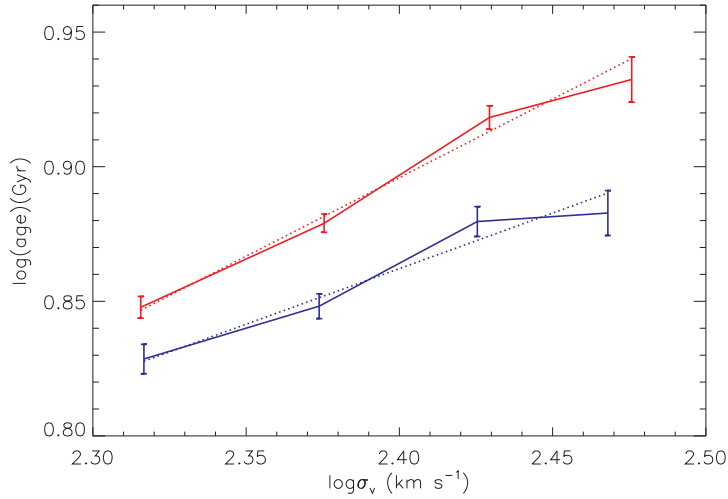


Fig. 9 Age- σ relation of LRGs. The top and bottom solid lines show the relations obtained from ULySS and STARLIGHT, respectively. The dotted lines respectively show the best fit to the age- σ relation of LRGs.

6.1 Age- σ Relation of LRGs

Figure 4 shows that the ages of LRGs increase with increasing velocity dispersions. We give a quantitative relation between age and σ below. Assuming that the increase of age with increasing σ follows a power law, i.e., $t_{\text{age}} \propto \sigma_v^\gamma$, then we average the ages and metallicities for each of the four sub-samples, and estimate γ by fitting the exponential relation using the mean ages and mean σ values from the four sub-samples. The final age- σ relations from fitting with ULySS (red line; $\gamma = 0.58 \pm 0.04$) and that from STARLIGHT (blue line; $\gamma = 0.41 \pm 0.06$) are shown in Figure 9. In the above fitting, however, the obtained ages of different galaxies may have different reference points since those galaxies are located at different redshifts. Here we correct this by converting the age of each galaxy at redshift z to that at redshift 0 by adding the lookback time of the galaxy at z . To do so, a flat Λ CDM cosmology is adopted, i.e., $H_0 = 70 \text{ km s}^{-1} \text{ Mpc}^{-1}$ and $\Omega_m = 0.30$. With these corrected ages, we refit the age- σ relation, and find $\gamma = 0.69 \pm 0.04$ and $\gamma = 0.56 \pm 0.05$ for the relations obtained from the fittings by ULySS and STARLIGHT, respectively.

Our results clearly show the dependence of age on σ for early-type galaxies, as was also revealed by a number of other studies. For example, Nelan et al. (2005) studied the age- σ relation of 4097 red-sequence galaxies in 93 low-redshift galaxy clusters, and derived a relation of $t_{\text{age}} \propto \sigma_v^{0.59 \pm 0.13}$; Smith et al. (2009) investigated a sample of 232 quiet galaxies in the Shapley super cluster of galaxies, and obtained a relation of $t_{\text{age}} \propto \sigma_v^{0.40}$. However, the estimates of γ seem to be slightly different in different studies, which might be due to different sample selection criteria, different treatments for emission lines, or different fitting methods, etc. (as discussed in Nelan et al. 2005).

6.2 Star Formation History of LRGs

The star formation history of LRGs can be reconstructed according to the SSPs obtained from the spectral fitting. We calculate statistics for x_j and μ_j from fitting every spectrum in our sample. First, we sum x_j and μ_j of all resultant SSPs with different metallicities but the same age to be the contribution of an SSP with this age to the flux and mass of observation at the normalization wavelength

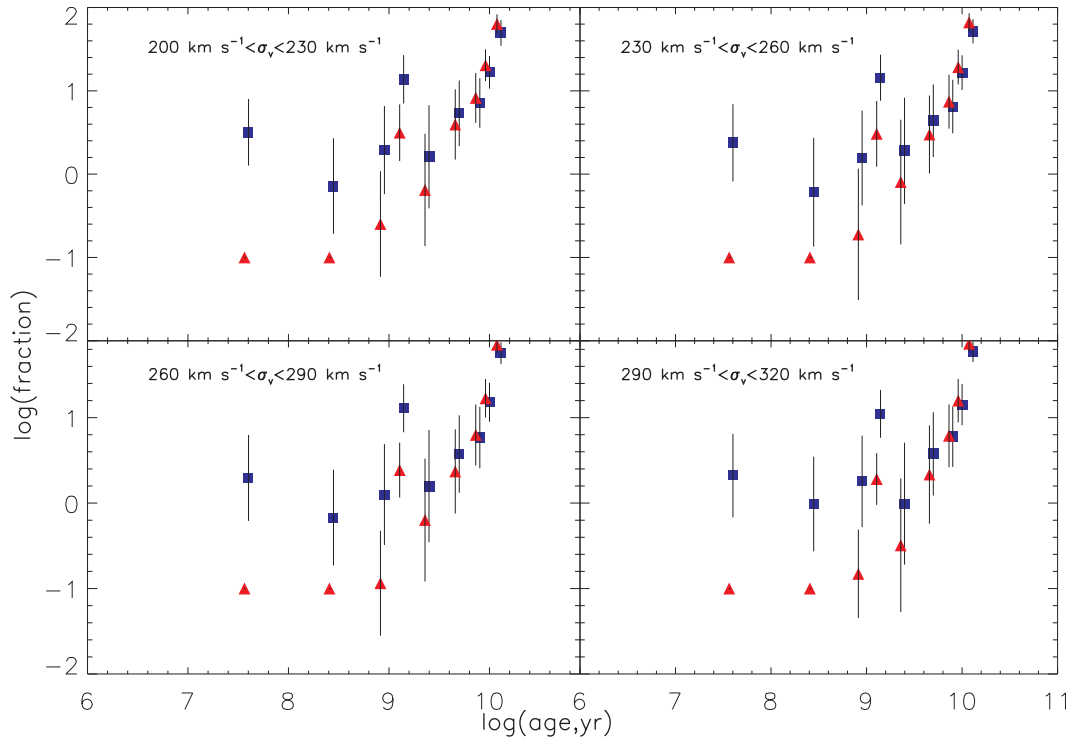


Fig. 10 Star formation history of LRGs. Squares and triangles represent the light-weighted and mass-weighted fraction, respectively.

($\lambda = 4020 \text{ \AA}$). Secondly, we calculate the mean and standard deviation for the summed x_j and μ_j in logarithmic coordinates. In terms of statistics, we show percentages of SSPs with different ages for each of the four sub-samples in Figure 10, which denote the light-weighted results as squares and the mass-weighted results as triangles. For a clear comparison, we plot the mass-weighted results with an offset of 0.04 along the horizontal axis. We only designate the upper limit of fractions of very young stellar populations (4, 286 Myr) because their contribution is quite small ($\leq 0.1\%$). Generally speaking, old stellar populations are the dominant component. In order to display distributions of light fractions and mass fractions of stellar populations with different ages, we divide the resultant nine SSPs into three groups of young stellar populations (YSP; ≤ 1 Gyr), old stellar populations (OSP; ≥ 2.5 Gyr) and intermediate-age stellar populations (ISP; $1 \sim 2.5$ Gyr). We calculate the light and mass fractions of YSP, ISP and OSP for every spectrum, and show the mass fractions (solid line) and light fractions (dashed line) of YSP, ISP and OSP for each of the four sub-samples in Figure 11.

From Figure 11, we can conclude that, for YSP, most have a mass fraction less than 1% and a light fraction less than 10%; for ISP, most have mass fractions less than 10% and have wide distributions of light fractions; for OSP, the majority have mass fractions of more than 90% and light fractions from 50% to 100%. On the whole, old stellar populations formed in an early period and less than 1% of mass formed in the low redshift universe constitute the dominant components in LRGs. All these conclusions completely agree with those from previous work (Cimatti et al. 2008; Spinrad et al. 1997; Thomas et al. 2010).

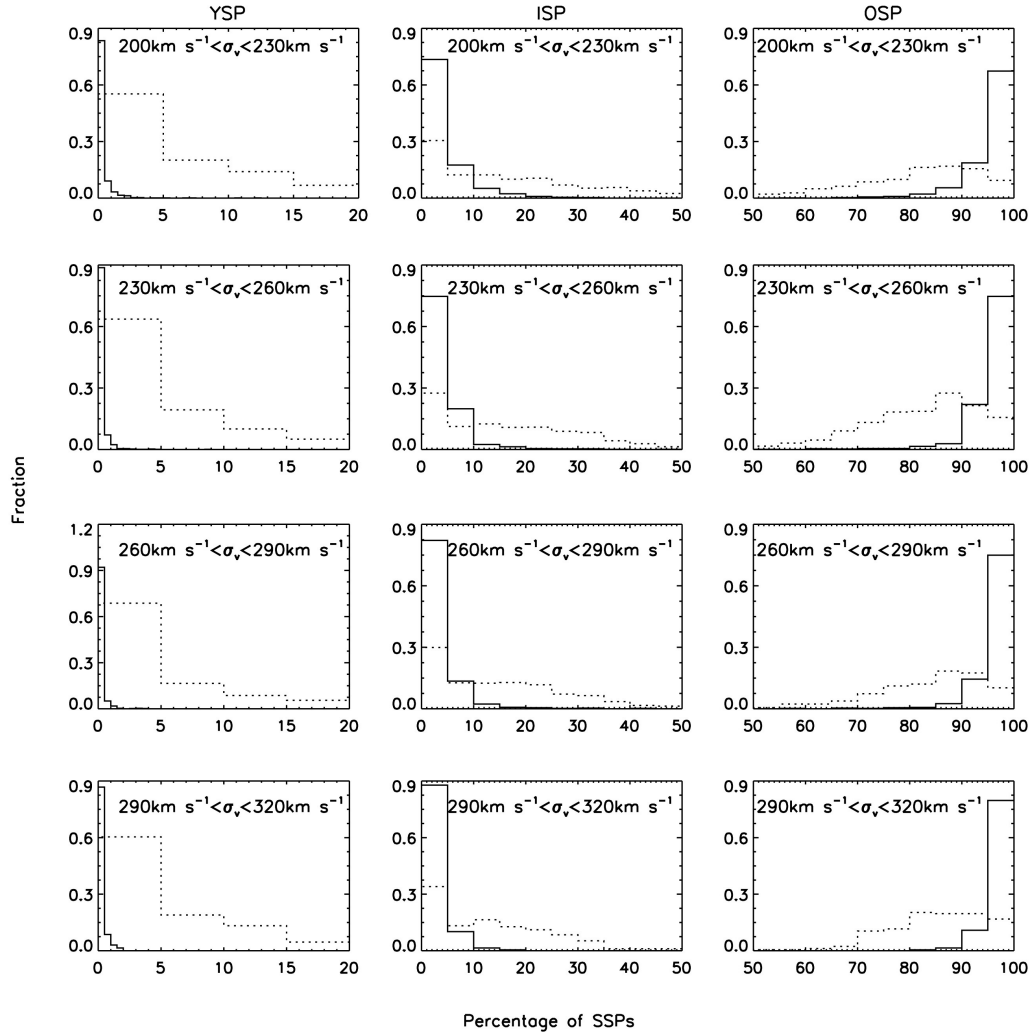


Fig. 11 The distribution of YSP, ISP and OSP for LRGs. The solid line and the dotted line represent the mass percentage and light percentage, respectively.

7 SUMMARY

We compare ULYSS and STARLIGHT by using them to simultaneously study the stellar populations of a sample of quiet LRGs selected from SDSS DR7. For those LRGs with high S/N spectra, the two packages can generally give consistent results, although ULYSS can give older ages and richer metallicities. For LRGs with low S/N spectra, results obtained from the fitting by ULYSS need to be checked carefully because ULYSS can easily become trapped in some local minima of parameter space. Based on the fitting results of high-S/N spectra, we further investigate the age- σ relation and star formation history of LRGs. We find that mass associated with the majority of LRGs formed at high-redshift, and the ages of LRGs increase with increasing velocity dispersion, which is consistent with the “downsizing” picture of galaxies formation.

Acknowledgements This work was supported by the National Natural Science Foundation of China (Grant Nos. 11033001 and 11073024).

References

- Abazajian, K. N., Adelman-McCarthy, J. K., Agüeros, M. A., et al. 2009, *ApJS*, 182, 543
Bertelli, G., Bressan, A., Chiosi, C., Fagotto, F., & Nasi, E. 1994, *A&AS*, 106, 275
Bruzual, G., & Charlot, S. 2003, *MNRAS*, 344, 1000
Chabrier, G. 2003, *PASP*, 115, 763
Chen, X. Y., Liang, Y. C., Hammer, F., et al. 2010, *A&A*, 515, A101
Cid Fernandes, R., Gu, Q., Melnick, J., et al. 2004, *MNRAS*, 355, 273
Cimatti, A., Cassata, P., Pozzetti, L., et al. 2008, *A&A*, 482, 21
Crampin, J., & Hoyle, F. 1961, *MNRAS*, 122, 27
Eisenstein, D. J., Annis, J., Gunn, J. E., et al. 2001, *AJ*, 122, 2267
Koleva, M., Prugniel, P., Bouchard, A., & Wu, Y. 2009, *A&A*, 501, 1269
Liu, G., Lu, Y., Chen, X., et al. 2012, *ApJ*, 758, 107
Nelán, J. E., Smith, R. J., Hudson, M. J., et al. 2005, *ApJ*, 632, 137
Smith, R. J., Lucey, J. R., & Hudson, M. J. 2009, *MNRAS*, 400, 1690
Spinrad, H., Dey, A., Stern, D., et al. 1997, *ApJ*, 484, 581
Thomas, D., Maraston, C., Schawinski, K., Sarzi, M., & Silk, J. 2010, *MNRAS*, 404, 1775